Advances in Water Resources 97 (2016) 224–232

Contents lists available at ScienceDirect

Advances in Water Resources

journal homepage: www.elsevier.com/locate/advwatres

Experimental study of 3D Rayleigh–Taylor convection between miscible fluids in a porous medium

Yuji Nakanishi, Akimitsu Hyodo, Lei Wang, Tetsuya Suekane*

Department of Energy Sciences, Tokyo Institute of Technology, 4259-G3-31, Nagatsuta, Midori-ku, Yokohama, 226-8502 Japan

ARTICLE INFO

Article history:
Received 8 February 2016
Revised 27 September 2016
Accepted 27 September 2016
Available online 30 September 2016

Keywords:
Natural convection
Rayleigh–Taylor instability
Mechanical dispersion
X-ray CT
Fingering structures

ABSTRACT

The natural convection of miscible fluids in porous media has applications in several fields, such as geoscience and geoengineering, and can be employed for the geological storage of CO_2. In this study, we used X-ray computer tomography to visualize 3D fingering structures associated with the Rayleigh–Taylor instability between miscible fluids in a porous medium. In the early stages of the onset of the Rayleigh–Taylor instability, a fine crinkling pattern gradually appeared at the interface. As the wavelength and amplitude increased, descending fingers formed on the interface and extended vertically downward; in addition, ascending and highly symmetric fingers formed. The adjacent fingers were cylindrical in shape and coalesced to form large fingers. The fingers appearing on the interface tended to become finer with increasing Rayleigh number, which is consistent with linear perturbation theory. When the Péclet number exceeded 10, transverse dispersion increased the finger diameter and enhanced the finger coalescence, strongly impacting the decrease in finger number density. When mechanical dispersion was negligible, the finger-extension velocity and the dimensionless mass-transfer rate scaled with the characteristic velocity and the Rayleigh number with an appropriate length scale. Mechanical dispersion not only reduced the onset time but also enhanced the mass transport.

1. Introduction

The natural convection of miscible fluids in porous media has applications in fields as diverse as carbon dioxide capture and storage (CCS) (Herzog, 2001; Huppert and Neufeld, 2014; Lindeberg and Wessel-Berg, 1997; Riaz and Cinar, 2014), petroleum engineering (Aziz et al., 1973), geothermal energy recovery (Barvier, 2002; Henley and Ellis, 1983; Oldenburg and Pruess, 1998), patterned ground (Gleason et al., 1986; Krantz, 1990), and the intrusion of saltwater into fresh water (Fernandez et al., 2002). Semi-infinite-fluid layers separated by a horizontal interface with the dense layer above the lighter layer can experience Rayleigh–Taylor instability (Kolditz et al., 1998). Small disturbances at the interface (such as those associated with thermal fluctuations) grow exponentially over time and eventually induce macroscopic convection (Heller, 1966). The Rayleigh–Taylor instability is a special case of fingering instability in vertical displacement flows (Homsy, 1987; Saffman and Taylor, 1958) in which the interface moves in the normal direction and competes with viscous and gravitational instabilities depending on the conditions (Coskuner and Bentsen, 1990; Manickam and Homsy, 1995; Tan and Homsy, 1986). Wooding (Wooding, 1969) observed the growth of fingers associated with the Rayleigh–Taylor instability in a Hele-Shaw cell and found that the mean wavelength grew proportionally to $t^{1/2}$ because adjacent fingers coalesced over time. Moreover, he observed that, at an advanced stage of development, the fingertips tended to become unstable and break into two separate fingers. Due to the opacity of porous media, most experimental studies have used Hele-Shaw cells or 2D porous media. At high Rayleigh numbers, *Ra*, significant gradients across the gaps of Hele-Shaw cell can develop (Kolditz et al., 1998).

For CCS applications (Herzog, 2001), mass transfer associated with natural convection has attracted considerable attention because it can strongly impact the time required to transit from the buoyant CO_2 state to dissolved CO_2, which does not pose a leak risk. Rayleigh–Taylor convection and Rayleigh–Bénard convection are simplified models of natural convection in porous media. In many studies (Cooper et al., 2014; Ennis-King and Paterson, 2005; Ennis-King and Paterson, 2007; Farajzadeh et al., 2007; Frykman and Wessel-Berg, 2014; Green and Ennis-King, 2013; Hassanzadeh et al., 2005; Hassanzadeh et al., 2006; Hassanzadeh et al., 2007; Hewitt et al., 2013; Hewitt et al., 2014; MacMinn et al., 2012; MacMinn et al., 2011; Neufeld et al., 2010; Pau et al., 2010; Szulczewski et al., 2013; Xu et al., 2006), natural convection in CCS has been modeled using Rayleigh–

* Corresponding author. Fax: 81+45-924-5575.
E-mail addresses: nakanishi.y.ag@m.titech.ac.jp (Y. Nakanishi), hyodo.a.aa@m.titech.ac.jp (A. Hyodo), wang.l.ah@m.titech.ac.jp (L. Wang), tsuekane@es.titech.ac.jp (T. Suekane).

http://dx.doi.org/10.1016/j.advwatres.2016.09.015
0309-1708/

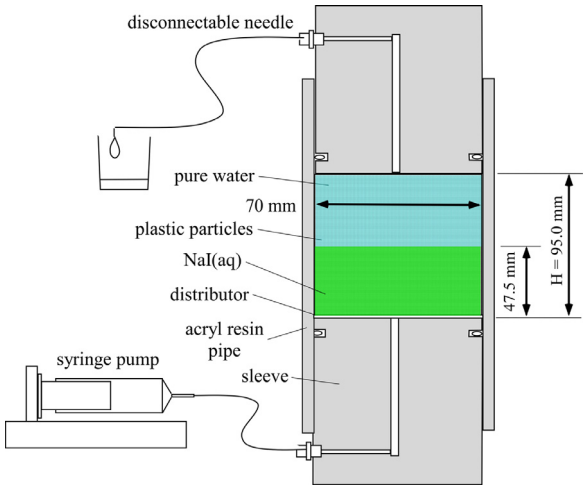

Fig. 1. Schematic of the experimental setup.

Bénard convection, where a porous medium has a finite height, and impermeable-boundary conditions have been imposed at the top and bottom boundaries. However, in some injection procedures, Rayleigh–Taylor convection may be induced in CO_2 reservoirs. Rayleigh–Taylor convection is an ideal situation with respect to Rayleigh–Bénard convection (Elder, 1968) because, in ideal Rayleigh–Taylor convection, the boundary conditions are imposed infinitely far from the initial interface (Hewitt et al., 2013). In the case of Rayleigh–Bénard convection, the dimensionless mass-transfer rate (i.e., the Sherwood number, *Sh*) is correlated with *Ra*. However, for Rayleigh–Taylor convection, little research has been conducted to provide insight into the mass-transfer properties.

In this report, we describe laboratory-scale experiments in which we applied X-ray computed tomography (CT) to visualize the 3D structures of fingers in a porous medium associated with the Rayleigh–Taylor instability. The effects of *Ra* on the finger structures and on the mass-transport properties are discussed. Moreover, we demonstrate that mechanical dispersion strongly affects the finger structure.

2. Experimental setup and procedures

2.1. Experimental setup

The recent rapid progress in X-ray CT enables 3D visualization of the evolution of finger structures with time. Melamine resin particles with average diameters, d_p, of 215 μm (180–250 μm; Ube Sand Engineering Co. Ltd.; XH series), 338 μm (250–425 μm), 513 μm (425–600 μm), 780 μm (530–1030 μm), and 975 μm (760–1190 μm) were packed into individual acrylic resin tubes with inner diameters of 70 mm (Fig. 1) to change the permeability, *k*. Prior to packing, the particles were rinsed well to remove any fine contaminants. After drying under laboratory conditions, the weighed particles were packed into 95-mm-high tubes to enable reproducibility in terms of *k* and porosity, φ (Table 1). The determined values of *k* based on the water-flooding experiments were approximately related to the average d_p such that $k = 5.10 \times 10^{-4}\ {d_p}^2$.

As the miscible-fluid pair, we used purified water and brine, i.e., purified water doped with sodium iodide (NaI) or a mixture of NaI and sodium chloride (NaCl; Table 2). Due to its high atomic number, iodide highly attenuates X-rays; however, if the density difference $\Delta\rho$ with respect to purified water increases upon doping with NaI, high X-ray attenuation induces a hardening effect, which is in fact an unphysical gradient of the CT value in the radial direction in reconstructed CT images and is caused by the partial saturation of attenuation for a certain range of X-ray wavelengths. To avoid this hardening effect, a substantial $\Delta\rho$ was achieved by combined doping with NaI and NaCl. Note that the X-ray attenuation of NaCl is considerably lower than that of NaI.

Table 1
Properties of porous media.

Average particle diameter d_p (μm)	Permeability* k, (m^2)
215 (180–250)	7.87×10^{-11}
338 (250–425)	1.30×10^{-10}
513 (425–600)	1.90×10^{-10}
780 (530–1030)	2.63×10^{-10}
975 (760–1190)	4.87×10^{-10}

* Permeability was determined based on water-flooding experiments.

Table 2
Properties of fluids.

Fluid pair	Concentration		Density difference	Viscosity†
	NaI (wt %)	NaCl (wt %)	$\Delta\rho$ (kg/m^3)	μ (μPa s)
A	5.26	0.00	52.6	1139
B	5.26	5.82	111	1262
C	5.26	12.3	176	1364
D	5.26	19.7	249	1507

† Viscosity was determined by using a falling-ball viscometer (Thermo Scientific HAAKE C) at 17 °C.

Table 3
Range of *Ra* in experiments.

Particle diameter	Fluid pair / density difference $\Delta\rho$ (kg/m^3)			
d_p (μm)	A	B	C	D
	52.6	111	176	249
215	3600 ■	6800 ■	10,100 ■	12,900 ■
338	6000 ▲	11,300 ▲	16,600 ▲	21,300 ▲
513	8700 ▼	16,500 ▼	24,300 ▼	31,200 ▼
780	12,000 ●	–	–	–
975	22,300 ♦	–	–	–

Consistent notation is used for all figures.

2.2. Experimental procedures

The experiments were conducted according to the following procedures. After packing the particles, the packed bed was saturated with purified water using a vacuum chamber. $\varphi = 0.470$ was estimated from the change in the weight, which occurred upon saturation with the purified water, for each value of d_p. Next, the brine was injected vertically upward into the packed bed such that, when using a syringe pump (KD scientific), the bottom half of the packed bed was saturated with brine at a constant flow rate. Because the displacement front was stabilized by gravity, the thickness of the interface δ was (10.9 ± 0.434) mm, which was estimated from the CT image, for all the experimental conditions shown in Table 3. Next, the packed bed was flipped upside down and set into the X-ray CT scanner (Comscantechno, ScanXmate-RB090SS). It took approximately 50 s to acquire 400 images from all directions. The scan continued once per minute until the natural convection was complete.

The CT values were adjusted so that the CT values for an acrylic resin tube and the surrounding air would be the same for all of the scans. Subsequently, the CT values were transformed into NaI concentrations using calibration curves, which were acquired in advance for each particle size. The reconstructed images consisted of 496 slice images of 496×496 pixels at a resolution of 193 μm/pixel in all directions.